Methods to determine hydration states of minerals and cement hydrates

Luis G. Baquerizo [a,*], Thomas Matschei [a], Karen L. Scrivener [b], Mahsa Saeidpour [c], Alva Thorell [c], Lars Wadsö [c]

[a] Innovation, Holcim Technology Ltd., CH-5113 Holderbank, Switzerland, [b] Laboratory of Construction Materials, Ecole Polytechnique Fédérale de Lausanne, CH-1015 Lausanne, Switzerland , [c] Building Materials, Lund University, Box 124, 221 000 Lund, Sweden.

Corresponding author:

* E-mail address: luis.baquerizoibarra@holcim.com Tel.: +41 58 858 64 31

Abstract

This paper describes a novel approach to the quantitative investigation of the impact of varying relative humidity (RH) and temperature on the structure and thermodynamic properties of salts and crystalline cement hydrates in different hydration states (i.e. varying molar water contents). The multi-method approach developed here is capable of deriving physico-chemical boundary conditions and the thermodynamic properties of hydrated phases, many of which are currently missing from or insufficiently reported in the literature. As an example the approach was applied to monosulfoaluminate, a phase typically found in hydrated cement pastes. New data on the dehydration and rehydration of monosulfoaluminate are presented. Some of the methods used were validated with the system Na_2SO_4–H_2O and new data related to the absorption of water by anhydrous sodium sulfate are presented. The methodology and data reported here should permit better modeling of the volume stability of cementitious systems exposed to various different climatic conditions.

Keywords

Cement hydrates; monosulfoaluminate; hydration states; thermodynamic properties; characterization techniques.

1. Introduction

1.1. General

Varying hydration states of minerals and hydrated phases and their associated changes in molar volume (i.e. density) is a common cause of failure in porous materials. Two mechanisms can be distinguished: i) crystals that can precipitate from a saturated solution and grow in confined spaces such as porous media due to changes in temperature and relative humidity RH and ii) hydrated minerals such as clays that can absorb or release water from their structure depending on the external conditions producing swelling or shrinkage directly without full dissolution and recrystallization.

The first mechanism, commonly called salt damage, is one of the main reported causes of failure in stones, cultural heritage buildings and any porous building material [1-3]. The growth of salts produces a crystallization pressure which can exceed the tensile strength of a porous material causing its rupture. Most cases of the damage are the consequence of unfavorable conditions of temperature and RH that result in repeated cycles of dissolution and crystallization, or hydration and dehydration [3]. Sodium sulfate is very well known for its ability to cause damage to porous media such as building stone. This is usually attributed to the growth of $Na_2SO_4 \cdot 10H_2O$ (mirabilite) from a supersaturated solution [1]. In relation to Portland cement-based concretes, the crystallization of ettringite due to external sulfate attack or autogenous delayed ettringite formation can cause complete failure of structures [4-5].

The second mechanism is related to the ability of layered minerals such as smectite clays and layered double hydroxides (LDH) to absorb or release water from the interlayer space depending on the external conditions, especially varying temperature and RH [6-7]. Ca^{2+}-montmorillonite, for instance, shows an increase of basal space d(001) from ~0.97 nm in the anhydrous state up to ~1.8 nm in the three-layer hydrate, which is associated with considerable changes in molar volume [8]. LDH are lamellar materials with positively charged layers and charge-balancing anions in the interlayer and they have many physical and chemical properties in common with those of clay minerals such as ion-exchange properties and swelling in water [7]. Several phases formed during hydration of cement belong to this family and each of these can exist in several different well-defined hydration states.

1.2. Hydration states of crystalline cement hydrates

Cement clinker phases react chemically with water to form cement hydrates. Some of these hydrates are crystalline phases with LDH- or ettringite-type structures. These so called Alumino-Ferrite mono- and tri-phases (AFm and AFt) show different hydration states depending on the temperature and relative humidity (RH) to which they are exposed, similar to what is observed in many clay minerals. Varying the hydration states of these phases can have a significant impact on the density of cement paste. The molar volume of some AFm phases can decrease by as much as 20% during drying [9], strongly influencing the porosity and performance of cementitious systems.

The most important AFm and AFt phases and their reported water contents are presented in Table 1. Water molecules can be incorporated in the interlayer in AFm phases (LDH-type) or in the

interchannel in AFt phases (ettringite type). In the case of AFm phases different types of interlayer water can be identified: water molecules strongly bound to the calcium cations of the main layer, and space filling water molecules which are lost first during an increase in temperature or a decrease in RH [10].

There is presently no systematic approach to assessing the stability range (as a function of temperature and RH) of cement hydrates which takes into account the impact of different hydration states. Moreover, a complete database of thermodynamic properties related to the absorption/desorption of water from the crystal structures of such hydrates is not yet available.

The aim of this study is to examine a set of characterization techniques intended for to the determination of the hydration states of minerals such as cement hydrates and see how these methods correlate with or complement each other. Some of the techniques studied have already been widely used, such as X-ray diffraction (XRD) and thermogravimetric analysis (TGA), but others, for instance the sorption balance technique and sorption calorimetry, are less well known. Subsequently, measurements and calculations of enthalpies related to the absorption/desorption processes are described using results from sorption calorimetry and from a novel hydrate pair - humidity buffer method that makes use of phase rule constraints [24-25]. A similar approach was used by Chou et al. to study the stability of hydrated sulfate salts [26-30]. The experimental results from sorption balance, sorption calorimetry and the hydrate pair - humidity buffer method were validated on the relatively well described system Na_2SO_4–H_2O, including the salts thenardite and mirabilite.

At the end of the paper the stability ranges of the different hydration states of monosulfoaluminate (Ms) are presented, as well as the thermodynamic properties associated with these changes. Monosulfoaluminate was chosen to test the methodology as it is one of the most common AFm cement hydrates which can make up to 10% by volume of a hydrated cement paste. This hydrate contains a sulfate anion (SO_4^{2-}) in its interlayer and exists in different hydration states.

2. Materials and conditioning

2.1. Reference material

The hydrate pair - humidity buffer method, the sorption balance and sorption calorimetry experiments were validated on thenardite and mirabilite: salts with known RH and temperature stability. Reagent grade thenardite was obtained from Sigma Aldrich, > 99% pure, and mirabilite $Na_2SO_4 \cdot 10H_2O$ was prepared by wetting thenardite with degassed and deionized water.

2.2. Cement hydrate preparation

All syntheses were done from analytical grade reagents. For the synthesis of monosulfoaluminate tricalcium aluminate (C_3A) and anhydrite were used as precursors. C_3A was prepared from a 3:1 molar ratio of $CaCO_3$ and Al_2O_3 at 1400°C, based on the procedure given by Matschei [31]. Anhydrite $CaSO_4$ was prepared by dehydration of gypsum in a muffle furnace at 550°C overnight. Double distilled CO_2 free water was used in the synthesis of the hydrates. Monosulfoaluminate $C_4A\hat{S}H_{14}$ was prepared by suspending a 1:1 molar mixture of C_3A and $CaSO_4$ with a water/solid

ratio (w/s) of 20 at 85 °C during 14 days in a PTFE bottle. Once purity has been confirmed by XRD, the solid was vacuum filtered under N_2 atmosphere in a glove box and subsequently aged at 25 °C (20 months) inside hermetically sealed glass bottles equilibrated at different RH using saturated salt solutions [32] as shown in Table 2. The RH was periodically checked using a Testo 174H humidity probe. Monosulfoaluminate synthesis was also carried out at 5°C to study the impact of low temperatures on the hydration states.

3. Experimental methods and analysis

3.1. X-Ray Diffraction (XRD)

This characterization technique was used to analyze the crystal structure, e.g. space group and lattice parameters of synthetic cement hydrates, as well as to identify possible impurities precipitated during the synthesis. Then, changes of the unit cell volume can be calculated when samples are exposed to different temperatures and RHs.

X-ray analyses of monosulfoaluminate wet and dried to different RHs were carried out at room temperature (unless otherwise stated) with a Bruker D8 Advance diffractometer (CuKα radiation, 45 mA, 35 kV) equipped with a Super Speed detector, in the 2θ range 5-70°, with a step size and time per step of 0.02° and 0.5 s, respectively. Samples were prepared inside a glove box filled with N_2. A low background- airtight specimen holder (Bruker AXS) was used to avoid carbonation and drying during testing. The peak profile and lattice parameters were determined by a LeBail fit [33] using TOPAS 4.2 (Bruker AXS). When the crystal structure of a specific hydration state was not known, assumptions such as space group and initial lattice parameters were made in order to obtain

relevant data. In the case of monosulfoaluminate the crystal structure of kuzelite was used as starting model [34].

In addition to conventional XRD, a humidity chamber CHC plus^{+} from Anton Paar coupled to a Bruker D8 Advance diffractometer (CuKα radiation, 45 mA, 35 kV) was used to determine lattice parameters of the lowest hydration state of monosulfoaluminate under dry N_2 flow at 90 °C.

3.2. Thermogravimetric analysis (TGA)

Thermogravimetry measurements were carried out with a Mettler Toledo TGA/SDTA 851^{e} under N_2 flux, over the temperature range 25-1200 °C with a heating rate of 20 K/min. Measurements were done on samples dried at different RH once the presence of a single hydration state was confirmed by XRD. This data enabled us to measure the water content of pure hydrates. Together with the volume information obtained by XRD, the density of a cement hydrate dried at a specific temperature and RH can be calculated.

3.3. Hydrate pair - humidity buffer method

This method was developed to determine the RH at which a change in hydration state occurs. It applies the salt-hydrate pair principle which considers a thermodynamic equilibrium between hydrate pairs, i.e. two hydration states of the same salt, and the water vapor pressure of the surrounding gas. Similar methods have been used before mainly as humidity calibrators [24] and to control RH in confined environments [25,35].

The technique is based on simple phase rule restrictions. Consider a chemical system with 2 components (C), a solid of chemical composition **A** and water H_2O. As shown in the imaginary RH/T phase diagram in Fig. 1, component **A** may take up water and exist with different hydration states x and y hence forming the phases **A**·xH_2O and **A**·yH_2O (consider that $x \geq 0$ and $y > x$) or dissolve to form a solution. If we consider the line *b* there are 3 phases (P) coexisting: **A**·xH_2O, **A**·yH_2O and water vapor. Using the phase rule the number of degrees of freedom (F) of the system is then 1 (F = C – P + 2; C=2; P=3 therefore F=1). Hence at every temperature the system will have a fixed vapor pressure (or RH). Under these conditions the system is buffered, which means that under isothermal conditions the RH of the system will not change as long as the 3 phases are present.

The thermodynamic properties of the de/rehydration process **A**·yH_2O↔**A**·xH_2O can be calculated as follows:

For the reaction

A·yH_2O (s) → **A**·xH_2O (s) + (y-x)H_2O(g), (1)

where s and g are solid and gas, respectively, the Gibbs free energy of reaction is given by:

$$\Delta G_r^o = -RT\ln K = -RT\ln\frac{a(\mathbf{A}\cdot x\mathrm{H_2O})\, a(\mathrm{H_2O})^{y-x}}{a(\mathbf{A}\cdot y\mathrm{H_2O})} \quad (2)$$

By defining the activity of all pure solid phases as 1, then:

$$\Delta G_r^o = -RT\ln[a(\mathrm{H_2O})^{y-x}] = (x-y)RT\ln[f(\mathrm{H_2O})] = (x-y)RT\ln\frac{f^*(\mathrm{H_2O})RH}{100} \quad (3)$$

where ΔG_r° is the standard Gibbs free energy of the reaction (1), *T* is the absolute temperature, *K* is the equilibrium constant, *R* is the gas constant, *a*(H_2O) is the activity of H_2O in vapor, *f*(H_2O) is the equilibrium fugacity, *f**(H_2O) is the fugacity of pure H_2O at *T* and *RH* is the equilibrium relative

humidity [27-30]. Since ln K can be calculated at any temperature for the reaction (1) according to Eq. (3) then the standard enthalpy of reaction $\Delta H_r°$ can be calculated with the van't Hoff equation:

$$\frac{\partial(lnK)}{\partial(1/T)} = -\frac{\Delta H_r^o}{R} \quad (4)$$

The standard entropy of reaction $\Delta S_r°$ can be calculated from the following equation:

$$\Delta G_r^o = \Delta H_r^o - T\Delta S_r^o \quad (5)$$

Experimentally a mixture of two phases with different hydration states was placed inside a small container (30 mL bottles of HDPE) and the RH at which the combined system reached equilibrium recorded with a tightly fitted pen hygrometer (Testo 605-H1, accuracy ± 3% RH). The hygrometer was tightened to the container by using a plastic cable gland thread PG16 which was also wrapped with Parafilm to avoid any leakage. Since the system is closed and there is no exchange of water with the exterior (diffusion of water through the bottle is negligible), the RH inside will be forced to be at equilibrium with the two hydrate phases at the given temperature. The same type of measurement can be made for a phase in equilibrium with its saturated aqueous solution (see line *a* Fig. 1). By varying the temperature during the experiments it is possible to assess phase boundary curves, which can then be used to construct RH-T phase diagrams. With Eqs. (3) – (5) the thermodynamic properties of the studied phases can be assessed.

3.4. Sorption balance

The sorption balance is commonly used in the pharmaceutical industry to study sorption behavior. In the present study a DVS Advantage (Surface Measurement Systems, London, UK) was used [37]. A schematic picture of this sorption balance is shown in Fig. 2. The mass of the small (5-100 mg)

sample is continuously measured with an analytical balance while it is exposed to a program which varies RH. The desired RH is reached by mixing different proportions of dry and water vapor saturated nitrogen gas streams. The accuracy of the generated RH is better than 1.5%.

With the sorption balance the mass of water taken up or released during a hydration/dehydration phase transformation or deliquescence and the water activity at which the process takes place can both be quantified. The mass is directly measured by the balance. To determine the water activity (RH/100) of a specific transformation one has to run either a ramp or a step method [38-39]. The step method is less sensitive to disturbances and less time consuming than the ramp method and therefore this regime was chosen for testing the samples. If the (constant) mass change rate dm/dt at each RH level is plotted as a function of the RH of the gas stream, a linear curve fit intersects dm/dt = 0 at the water activity at which an absorption/ desorption process takes place.

3.5. Sorption calorimetry

This technique provides the means to continuously scan water activity of a small sample, while simultaneously measuring water activity, moisture content and sorption enthalpy during an ad/absorption process.

The double twin isothermal sorption calorimeter used in this study is described in detail elsewhere [40]. It has two measuring positions placed 90 mm apart. The ampoule where the diffusion-sorption process takes place is schematically shown in Fig. 3. When introduced into the calorimeter, thermal power of evaporation (P_{vap}) and thermal power of sorption (P_{sorp}) are continuously measured by two twin microcalorimeters at the top and bottom chambers of the ampoule, respectively. The dry sample

is loaded in the bottom chamber, after which water is injected in the top and is transported by diffusion to the sample during the measurement. The diffusion rate depends on the geometry of the connecting tube and the water activity over the sample. The water diffusion rate, and thus the rate of change of moisture content of the sample, is proportional to P_{vap}. The water activity is calculated from the evaporation rate, and the mixing enthalpy is calculated by comparing the thermal powers of sorption and vaporization (more details about the method can be found in [41]).

The Enthalpy measured from the sorption microcalorimeter is normally presented as a mixing enthalpy, i.e., the difference between the enthalpy of the sorption process and that of condensation of liquid water. The mixing enthalpy can be seen as an "excess enthalpy" indicating how much additional heat is obtained from a sorption process compared to condensation of water. Sorption enthalpy, condensation enthalpy and the mixing enthalpy are related as follows:

$$\Delta H_{sorp} = \Delta H_{cond} + \Delta H_{mix} \quad (6)$$

Note, that the sorption enthalpy and the mixing enthalpy are properties of the moisture state at which the sorption/mixing takes place, while the condensation enthalpy of water is constant under isothermal conditions with a value of -2440 J/g H_2O at 25 °C. The thermodynamic sign convention used in this work states that processes are considered from the system viewpoint, i.e., if heat is lost by the system to the surroundings (heat is produced) the enthalpy change is negative. Enthalpies of sorption, condensation and mixing are therefore all negative.

4. Results

4.1. Validation

Before testing cement hydrates the hydrate pair - humidity buffer method, sorption balance and sorption calorimetry were validated with the system Na_2SO_4-H_2O which is relatively well described in the literature.

4.1.1. Hydrate pair - humidity buffer method

Consider the RH/T phase diagram of the system Na_2SO_4-H_2O as shown in Fig. 4 taken from Linnow [36]. Phase boundaries are shown with the lines *a, b* and *c*. Line *b* is the boundary between thenardite (Na_2SO_4) and mirabilite ($Na_2SO_4 \cdot 10H_2O$), both of them in the solid state. Above and below this line $Na_2SO_4 \cdot 10H_2O$ and Na_2SO_4 are the stable phases, respectively, but both phases can coexist on the line. The dotted line corresponds to a solution in metastable equilibrium with respect to thenardite and supersaturated with respect to mirabilite [1]. To validate the method three different mixes were prepared: one mix of 80%-20% thenardite - mirabilite and two mixes of 50%-50%. A few measurements were done using saturated solutions in order to measure the solid-liquid lines *a* and *c*. The measured RH for the thenardite-mirabilite equilibrium (filled dots) as well as the mirabilite or thenardite - saturated solution phase boundaries (open dots) are shown in Fig. 4, respectively. As can be seen there is good agreement with the phase diagram published by Linnow [36], which is based on thermodynamic data of aqueous Na_2SO_4 and the crystalline phases. Measurements done at around 5 °C on the thenardite-mirabilite boundary were rather scattered which might be due to low accuracy of the hygrometers at low temperature or the occurrence of other metastable equilibria including Na_2SO_4(III) and $Na_2SO_4 \cdot 7H_2O$ [3]. Since the purpose of this work was not to study in the

detail the equilibrium of the system Na_2SO_4-H_2O no further analysis was carried out in these samples.

In a next step the related thermodynamic relations are cross-checked. For the reaction:

$$Na_2SO_4 \cdot 10H_2O(s) \rightarrow Na_2SO_4(s) + 10H_2O(g) \quad (7)$$

mirabilite thenardite

The Gibbs free energy of reaction was calculated according to Eq. (3):

$$\Delta G_r^o = -RT\ln[a(H_2O)^{10}] - 10RT\ln\frac{f^*(H_2O)RH}{100} \quad (8)$$

Fig. 5 shows the relation between ln$K$ and 1/T. The error considered in the graph is due to the accuracy of the hygrometer (± 3%) and the plotted 95% prediction bands were calculated using Origin Pro 8.5. Finally, ln$K$ can be obtained at any temperature according to the following equation:

$$\ln K(\pm 0.8) = 174.2 - \frac{62797.0}{T} \quad (9)$$

The standard enthalpy of reaction $\Delta H_r°$ was calculated with help of the van't Hoff equation (Eq. (4)) using the slope value $\partial(\ln K)/\partial(1/T)$ obtained from Fig. 5. The standard entropy of reaction $\Delta S_r°$ was calculated from Eq. (5). Finally the calculated values of $\Delta G_r°$, $\Delta H_r°$ and $\Delta S_r°$ for reaction (7) are summarized in Table 3. The results are in very good agreement with previously reported values although the uncertainty in our data is probably larger in comparison to other techniques when we take the accuracy of the hygrometer as given by the manufacturer (+/-3% RH) into account. Nevertheless the results underline that even with the use of a simple experimental setup, as used here, it is possible to derive relatively complex phase diagrams and related thermodynamic data.

4.1.2. Sorption balance

To validate the operation of the sorption balance, Na_2SO_4 powder vacuum dried at 100 °C for 24 hours was used. The measurements were carried out at 25°C. Fig. 6a and b show the applied RH ramp program and the related evolution of sample mass, respectively. From 0% to 85% RH no water was absorbed by the sample. At RH >85% we observed a linear mass increase, corresponding to a constant water uptake rate. During drying a linear mass decrease was observed at RH< 85%. In Fig. 6c the mass change rate versus time is plotted and dm/dt at the final 10 min of each step was used to derive Fig. 7. The line fitted to these points passes $dm/dt = 0$ at a RH of 88.3%, which means that Na_2SO_4 absorbs water vapor until the sample reaches a metastable equilibrium with its saturated solution at a water activity of about 0.88 or 88% RH rather than precipitating as mirabilite, despite an obvious supersaturation with respect to this phase. This value is in agreement with the 87% RH shown in Fig. 4 (metastability line). Since no equilibrium was reached in any of the set RH the sorption isotherm could not be plotted.

4.1.3. Sorption calorimetry

The validation experiments were conducted at 25 °C on sodium sulfate dried as described in the previous section. Two measurements were carried out using different sample sizes.

Fig. 8 shows that both the sorption isotherm and the mixing enthalpy plot can be divided into two parts. First there is a constant water activity that ends at a moisture content of about 2.0 g H_2O/g Na_2SO_4; secondly a process with gradually increasing water activity. Note that the water activity

only changes a few tenths of a percent during the period of constant water activity. Fig. 8 can be interpreted as follows:

- The initial water activity is ~0.87 (or 87% RH) in both measurements and this is in agreement with both the literature [3,36] and the sorption balance measurement done in this study for a solution in metastable equilibrium with respect to thenardite (supersaturated with respect to mirabilite) (the dotted line in Fig. 4). Thenardite is thus dissolved to form a (metastable) saturated solution, similar to what happens at equilibrium above 32 °C where mirabilite is not stable.
- The moisture content increases at constant water activity up to a value of about 2.0 g H_2O/g Na_2SO_4 or 3.52 mol Na_2SO_4/kg H_2O, which agrees with the reported solubility of thenardite [3,43].
- The mixing enthalpy for a dissolution process should be constant and the measurement on the larger sample indicates that the value is about -125 J/g H_2O. The measurement on the smaller sample shows a drifting value, possibly because as the dissolution of the thenardite particles proceeds, a thicker and ticker layer of saturated solution is formed, the outer parts of which are more dilute (also seen in the slight increase in the water activity during the measurement). We have not found any values in literature to validate this metastable dissolution enthalpy.
- At moisture contents above about 2.0 g H_2O/g Na_2SO_4 the water activity starts to shift to higher values. At this point the last thenardite crystals have dissolved and as the measurement continues, the solution gets increasingly more and more diluted by the absorption of water. This is substantiated by the fact that the sample is a transparent liquid after the measurement. At a moisture content of 3.0 g H_2O/g Na_2SO_4, where the measurement on the smaller sample ends,

the system is still within the supersaturated region of the phase diagram with respect to mirabilite. However, there is no indication that any mirabilite forms during our measurements.

- Above a moisture content of 2.0 g H_2O/g Na_2SO_4 the measured enthalpy is due to the dilution of the aqueous solution. At increased moisture contents this will approach zero (pure water). Note the step in the mixing enthalpy from about -120 to -60 J/g H_2O when the last thenardite crystal is dissolved.
-

The three measured parameters have quite different errors. The moisture content is the most robust result, while the measurement of water activity can be disturbed by slow kinetics of absorption in some systems – even if this does not seem to be the case for the present measurements. The mixing enthalpy results become increasingly more uncertain at high RHs. Although we cannot at present make confident uncertainty calculations, a tentative estimate is that the error of the mixing enthalpies is at least ±10, ±20, and ±30 J/g H_2O at 80, 90 and 95% RH, respectively.

4.2. Results of monosulfoaluminate measurements

During cement hydration C_3A reacts with calcium sulfate (gypsum, hemihydrate or anhydrite) to produce ettringite, which subsequently reacts with the remaining C_3A to form monosulfoaluminate, an LDH-type AFm phase. This cement hydrate is known to present different hydration states and have a characteristic hexagonal morphology as shown in Fig. 9. In this section the results obtained on synthetic monosulfoaluminate (Ms) using the aforementioned characterization techniques are presented.

4.2.1. XRD and TGA

As shown in the X-ray diffractograms in Fig. 10 at 25 °C, Ms14 (the index 14 gives the water content of the phase in moles) is the hydration state observed under saturated conditions (100% RH) but it dehydrates at 97% RH to Ms12 which is found until 23% RH (the water content of Ms12 was verified by TGA, see Fig. 12). At 8% RH an even lower hydration state appears, which according to Dosch et al. [14] corresponds to Ms10, but according to our TGA results it is more likely to be Ms10.5, which agrees with results presented by Pöllmann [13]. An additional lower hydration state was obtained by vacuum drying the sample. According to TGA measurements this corresponds to Ms9. Since this hydration state tends to rehydrate fast at RH > 2%, XRD measurements were done using a sample dried in situ at 90 °C under N_2 flux in the humidity chamber. As no other hydration state was observed from 25 °C to 90 °C during the in-situ drying we assumed that this hydration state is the same one observed close to 0% RH at room temperature during vacuum drying. The exact RHs at which changes of hydration states take place were determined using sorption balance, sorption calorimetry and the hydrate pair - humidity buffer method, which gave comparable results.

An adsorption experiment was carried out after the desorption experiment, as shown in Fig. 10. After 1 year exposure of Ms10.5 to 23% and 33% RH, respectively, rehydration to Ms12 is only observed at 33% RH. Also when Ms12 is rewetted (immersed in water) it does not rehydrate to Ms14 at 25 °C. This hysteretic behavior will be further discussed in the coming sections.

In order to study the stability of Ms14 a series of in situ tests using the humidity chamber were carried out at temperatures >50 °C and high RHs. Rehydration Ms12→Ms14 takes place at around 90, 85 and 78% RH at 50, 65 and 75 °C.

A water rich hydration state was obtained by wet synthesis at 5 °C. According to several references it corresponds to Ms16 [13-14]. Nevertheless, most of the time the sample contained traces of Ms14, making the study of its stability difficult. For this reason, and because Ms16 was never observed from 25 °C to 85 °C in wet conditions, this hydration state was not considered during our stability and thermodynamic properties derivation analysis.

Attempts to index the diffraction patterns of the different hydration states were unsuccessful due to impurities, mainly small traces of ettringite and carbonates. For this reason the structure used for the refinement of the different hydration states of monosulfoaluminate was the kuzelite refined crystal structure published by Allmann [34] (ICSD# 100138, PDF# 41-0477) using the LeBail method [33]. The refined lattice parameters and volume of the different hydration states of monosulfoaluminate are given in Fig. 11. Ms16 refined lattice parameters are also included in this graph. It is worth noting that a decrease of RH can often lead to a very significant reduction in molar volume, in this case (i.e. for Ms14→Ms9) approximately 17% as shown in Fig. 11.

Fig. 12 shows the TGA curves of four different hydration states of monosulfoaluminate. The derivative plot shows similar weight losses at temperatures > 175 °C. The main differences are observed below this temperature. Ms12 shows two well defined water losses at 90 °C and 140 °C and Ms10.5 only a single water loss at 140 °C. In order to verify the water content of Ms14, a TGA test was carried out on a sample dried at 97% RH for two months. Unfortunately the sample was composed of Ms14+Ms12, so, for this reason, and because a considerable amount of condensed water is also present in the sample at this RH, it was not possible to determine the precise water

content of this hydration state. A similar problem occurred for Ms16. It was therefore simply assumed that the widely reported water contents of Ms14 and Ms16 were correct.

4.2.2. Hydrate pair - humidity buffer method

This method was used to determine the equilibrium Ms10.5-Ms12 according to the reaction:

$C_4A\hat{S}H_{12}(s) \rightarrow C_4A\hat{S}H_{10.5}(s) + 1.5H_2O(g)$ or

$$\text{Ms12(s)} \rightarrow \text{Ms10.5(s)} + 1.5H_2O(g) \quad (10)$$

Experimentally a mixture of Ms10.5 and Ms12 was placed inside a small container and the equilibrium RH at different temperatures was recorded. The measurements were repeated 3 times for each RH point at the same temperatures from 19 °C to 50 °C in order to obtain representative results. One of the mixes was rejected due to large differences in recorded RH, probably due to leakage during the testing. The accuracy of the hygrometers (± 3% RH) was considered in the graphs and in the calculations. A diagram presenting the measured critical RH of phase transition between Ms10.5 and Ms12 as function of temperature is shown in Fig. 13.

For reaction (10) we can write:

$$\Delta G_r^o = -RT\ln K = -RT\ln[f(H_2O)^{1.5}] = -1.5RT\ln\frac{f^*(H_2O)RH}{100} \quad (11)$$

From Eq. (11) and the data presented in Fig. 13 a linear van't Hoff plot (Fig. 14) can be derived. Then ln K follows Eq(12):

$$\ln K(\pm 0.1) = 26.2 - \frac{9895.8}{T} \quad (12)$$

The standard thermodynamic properties $\Delta G_r°$, $\Delta H_r°$ and $\Delta S_r°$ were calculated using Eqs. (3), (4) and (5), respectively and are shown in Fig. 14. The values are positive because reaction (10) shows a dehydration process; however, assuming a rehydration process these values would be negative.

4.2.3. Sorption balance

A sorption balance measurement was carried out on a monosulfoaluminate sample aged at 33% RH for 12 months, thus the initial hydration state was Ms12. The sample (10.1 mg) was initially equilibrated at 30% RH, followed by a desorption down to 0% RH, absorption up to 97% RH and finally desorption down to the initial state (30% RH). The test lasted about 92 hours and the RH at each step was kept constant during 2 to 3 hours (12 hours in the case of 0% RH). In contrast to the validation test done on Na_2SO_4 a constant mass was achieved in almost all the steps during this experiment and thus the mass change rate could not be used to determine the RH at which a change of hydration state took place. Nevertheless we could determine the complete sorption isotherm (Fig. 15) which is also useful to determine sudden changes of mass and thus of hydration states.

4.2.4. Sorption calorimetry

A sorption calorimetry measurement was done on monosulfoaluminate at 25 °C. The sample was initially vacuum-dried for 24 hours at room temperature, which means that at the beginning of the test the hydration state was Ms9 (as found by TGA). The initial mass of the sample was 89.6 mg.

Two hydration processes were observed (labelled 1 and 2 in Fig. 16). The calculated sorption isotherm is shown in Fig. 16 and is in good agreement with the isotherm measured by sorption balance.

Process 1 refers to the hydration step of Ms9 to Ms10.5 which is in very good in agreement with the sorption balance measurements. Stoichiometrically this process can be described by the following reaction:

$$Ms9(s) + 1.5H_2O(g) \rightarrow Ms10.5(s) \quad (13)$$

This process starts and finishes in the points *a* and *b*, respectively (see Fig. 16). As the hydrate pair – humidity buffer method could not be used to calculate the thermodynamic properties of this reaction/process, the experimental findings of the calorimetry measurements shows that the critical RH for the transformation of Ms9 to Ms10.5 is at around 2%RH. Thus the Gibbs free energy of reaction $\Delta G_r°$ of reaction (13) can be calculated according to Eq. (3), giving a value of 27.3 kJ/mol. As shown in Figure 17 the mixing enthalpy of this process is not completely constant, having an average value of -1365 J/g H_2O. The related sorption enthalpy ΔH_{sorp} for reaction (13) can now be calculated according to Eq. (6):

$$\Delta H_{sorp} = \Delta H_{cond} + \Delta H_{mix} = -2440\ \mathrm{J/g\ H_2O} - 1365\ \mathrm{J/g\ H_2O} = -3805\ \mathrm{J/g\ H_2O} = -68.6\ \mathrm{kJ/mol\ H_2O}$$

Since 1.5 moles of H_2O are needed to complete the hydration reaction (13), the total standard enthalpy of this reaction can be calculated as:

$$\Delta H_r^o = -68.6\ \mathrm{kJ/mol\ H_2O} \times 1.5 = -102.8\ \mathrm{kJ/mol}$$

Process 2 follows the hydration reaction (14):

$$Ms10.5(s) + 1.5H_2O(g) \rightarrow Ms12(s) \quad (14)$$

This reaction was also studied with the invariant point method. As seen in Fig. 16 this process starts in point *b* and finish approximately in point *c* where the mixing enthalpy is close to zero. The mixing enthalpy of this second process is around -670 J g^{-1} H_2O in the constant region. Following the same procedure as shown in Process 1 the corresponding standard enthalpy of reaction (14) is:

$$\Delta H_{sorp} = \Delta H_{cond} + \Delta H_{mix} = -2440 \text{ J/g } H_2O - 670 \text{ J/g } H_2O = -3110 \text{ J/g } H_2O$$

$$= -56.0 \text{ kJ/mol } H_2O$$

$$\Delta H_r^o = -56.0 \text{ kJ/mol } H_2O \times 1.5 = -84.0 \text{ kJ/mol}$$

This value is in good agreement to the enthalpy of reaction calculated from the invariant point method, 82.3 kJ/mol. Please note that the enthalpy value calculated with sorption calorimetry is negative because the test measures an absorption process which is exothermic.

In addition to processes 1 and 2, an endothermic process followed by an exothermic peak is observed after point *c*. As there is no significant increase in moisture content corresponding to this event, it seems that it has its origin in, for example, a conformational/ morphological change that may be initiated by the increase in moisture content, but does in itself not involve uptake of water. It should be noted that although the thermal effect of this event is clearly seen, the uncertainty in the absolute values increases significantly at high RH; thus the increase of the mixing enthalpy to positive values after the sharp exothermal peak is probably an artefact as the RH then approaches 100%.

It is worth noticing the very good agreement between the sorption isotherm measured on monosulfoaluminate by sorption balance and the one calculated one by sorption calorimetry as shown in Fig. 16. This clearly shows the power and reliability of this technique, which can also be used to study ad/absorption processes in salts, minerals, proteins, pharmaceutical products, etc.

4.2.5. Summary of results

A summary of results obtained for monosulfoaluminate is shown in Fig. 17 and Table 4. The hysteretic behavior observed in the sorption balance and XRD measurements is represented by a dashed-line. In the experimental studies Ms12 is observed when Ms14 is dried at 97% RH, for this reason the dehydration process Ms14 → Ms12 was assumed to take place at this RH. The rehydration Ms12 → Ms14 at 25 °C was not observed by any of the techniques used in this study. Thermodynamic properties of Ms16 found at 5 °C in wet conditions were not calculated due to lack of data. The density values of the different hydration states of monosulfoaluminate are shown in Table 5 and were calculated with Eq. (15):

$$D = ZM/N_A V \quad (15)$$

where D is the density, Z is the number of formula units per unit cell (which is 1.5 in our case), M is the molecular weight of the hydration state, V is the unit cell volume obtained from the XRD lattice parameters refinement and N_A is the Avogadro's number.

5. Discussion

5.1. Correlation between the methods and accuracy

The complementarity of the different methods shown in this work is evident. While XRD and TGA provide important structural data about the different hydration states, they cannot derive information about critical de/rehydration RH and thermodynamic properties. These were instead obtained by sorption calorimetry, sorption balance and the hydrate pair – humidity buffer method.

Sorption calorimetry was demonstrated to be a powerful tool which can give an almost complete thermodynamic description of a sorption process, although part of a measurement or a whole measurement may take place at metastable conditions. This has to be kept in mind when such experiments are evaluated. When calculating thermodynamic properties with the hydrate pair - humidity buffer method one has to consider that the accuracy of this method is determined by the hygrometers used to record RH and thus it is recommended to crosscheck the results with, for instance, sorption calorimetry measurements. Nevertheless average values calculated agrees well with previously reported data on Na_2SO_4, so despite the accuracy issue the hydrate pairs – humidity buffer method proved to be a simple, reliable and fast technique to determine stability ranges of different hydration states of minerals and thermodynamic properties of de/rehydration.

5.2. Interactions between Na_2SO_4 and water vapor

Na_2SO_4 (thenardite) and $Na_2SO_4 \cdot 10H_2O$ (mirabilite) were used to validate sorption balance, sorption calorimetry and the hydrate pair - humidity buffer method. The thenardite - mirabilite equilibrium RH as function of temperature and the enthalpy of reaction (7) determined by the humidity buffer method was in agreement with previously published data.

However, during sorption balance and sorption calorimetry tests the critical RH at which the first absorption process occurred on thenardite was about 87% RH (no water was absorbed below this RH) which corresponds to a solution in metastable equilibrium with respect to thenardite and supersaturated with respect to mirabilite [1,3,36]. The presence of a solution at the end of the calorimetry test confirmed the dissolution of thenardite during the measurement. This means that during an absorption process thenardite will tend to dissolve into a metastable solution with no precipitation of mirabilite. This behavior was also observed by Rodriguez-Navarro et al. [2] with in situ environmental scanning electron microscopy (ESEM) showing no hydration of thenardite into mirabilite but dissolution; during drying they observed crystallization of both thenardite and mirabilite. It has to be considered that our absorption tests took place under unconstrained conditions in a free non-confined space, opposite to what happens in real conditions where the deliquescence and crystallization of salts happen in porous media such as stone and building materials. In those cases a reduction of water activity and different supersaturation levels due to pore size can alter the dissolution behavior observed in our tests and mirabilite might precipitate upon hydration of thenardite.

At the end of the first absorption process at 87% RH (as measured by sorption calorimetry) the sample has absorbed 2g H_2O/g Na_2SO_4, which agrees perfectly with reported values of thenardite solubility [3,43]. The second process observed in the sorption calorimetry test, which starts once all the initial salt has been dissolved, is dilution of the initially saturated solution into a more and more dilute solution. This shows a lower mixing enthalpy compared to the dissolution process. Unfortunately, we have not found literature values to compare our enthalpy results because of the metastable nature of the processes.

5.3. Interactions between LDH-type cement hydrates and water vapor

Five hydration states of monosulfoaluminate were found in this study: Ms16, Ms14, Ms12, Ms10.5 and Ms9. Ms14 is stable under saturated conditions over 20°C and once it dehydrates to Ms12 it does not rehydrate to Ms14 at room temperature. Ms9 was obtained at a water activity close to zero. A hysteresis in the equilibria Ms10.5-Ms12 and Ms12-Ms14 was observed with XRD and sorption balance measurements, probably due to kinetic constraints or crystal size; it is believed that the larger the crystal size the longer it would take to absorb water within the structure. Another possibility for the hysteretic behavior is a related activation energy of de/rehydration which might be needed to remove/introduce water within the hydrate. In minerals such as clays, hysteresis can occur due to a non-reversible orderliness due to changes that occur in the structure of the material while water is being absorbed [45]. However during the hydrate pair – humidity buffer method the equilibrium RH between Ms10.5 and Ms12 agrees with the adsorption regime. This suggests that the adsorption results correspond to the real equilibrium between two coexisting hydration states. Enthalpy of sorption for the reaction Ms9→Ms10.5 was calculated from sorption calorimetry results, while the reaction Ms10.5→Ms12 was evaluated from both sorption calorimetry and the humidity buffer method, resulting in similar values. The sorption isotherms measured with sorption balance and sorption calorimetry were qualitatively and quantitatively similar. A water rich hydration state, Ms16, was found in wet conditions at low temperatures (5 °C) by XRD. Thermodynamic properties of the dehydration for the reaction Ms16→Ms14 were not calculated due to lack of stability even in wet state. Our research indicates that Ms16 can occur at low

temperatures, which agrees with observations done by Dosch et al. [14]. Further research is required to find out under which conditions this hydration state is stable.

The results clearly show the impact of drying condition on crystalline cement hydrates. At room temperature monosulfoaluminate will decrease about 17% in volume from Ms14 to Ms9. Although in real conditions the dehydration Ms14→Ms12 can occur, it is unlikely for a concrete structure to reach humidities where Ms10.5 and Ms9 are stable, 28.5% and 2% RH, respectively. Nevertheless, these low humidities are easily obtained during sample preparation prior to characterization, which includes vacuum drying, P-drying, solvent exchange and so on, which highlight the importance of our results in connection to the analysis of a hydrated cement paste.

5.4. Practical implications

The thermodynamic properties obtained on monosulfoaluminate are the first to be reported. This methodology will be subsequently used to derive stability conditions and thermodynamic properties of the different hydration states of the most important AFm and AFt phases present in ordinary Portland cement (OPC) and calcium aluminate cement (CAC) blended systems. This data will enable the modelling of the mineralogy and volume changes of a hydrated cementitious system exposed to different drying conditions. This opens the possibility to engineer cement mixes containing hydrate phase assemblages which are less sensitive to changing exposure conditions which can positively impact the performance and durability of cement based materials.

Acknowledgements

The research leading to these results has received funding from the European Union Seventh Framework Programme (FP7 / 2007-2013) under grant agreement 264448. We would like to thank Holcim Technology Ltd. for actively promoting cement research, especially the Innovation Function and the Analytical Lab of the Cement Manufacturing Function.

References

[1]. R. Flatt, Salt damage in porous materials: how high supersaturations are generated, J. Cryst. Growth. 242 (2002) 435-454.

[2]. C. Rodriguez-Navarro, E. Doehne, E. Sebastian, How does sodium sulfate crystallize? Implications for the decay and testing of building materials, Cem. Concr. Res. 30 (2000) 1527-1534.

[3]. M. Steiger, S. Asmussen, Crystallization of sodium sulfate phases in porous materials: The phase diagram Na_2SO_4–H_2O and the generation of stress, Geochim. Cosmochim. Acta. 72 (2008) 4291-4306.

[4]. M. Collepardi, A state-of-the-art review on delayed ettringite attack on concrete, Cem. Concr. Compos. 25 (2003) 401-407.

[5]. H.F.W. Taylor, C. Famy, K.L. Scrivener, Delayed ettringite formation, Cem. Concr. Res .31 (2001) 683-693

[6]. F. Bergaya, G. Lagaly, Chapter 1 - General Introduction: Clays, Clay Minerals, and Clay Science, in: F. Bergaya, G. Lagaly (Eds.), Developments in Clay Science, Elsevier, 2013, pp. 1-19.

[7]. C. Forano, U. Costantino, V. Prévot, C. Taviot Gueho, Chapter 14.1 - Layered Double Hydroxides (LDH), in: F. Bergaya, G. Lagaly (Eds.), Developments in Clay Science, Elsevier, 2013, pp. 745-782.

[8]. M.F. Brigatti, E. Galan, B.K.G. Theng, Chapter 2 - Structure and Mineralogy of Clay Minerals. in: F. Bergaya, G. Lagaly (Eds.), Developments in Clay Science, Elsevier, 2013, pp. 21-81.

[9]. L. Baquerizo, T. Matschei, K. Scrivener, The impact of water chemical potential on the hydration states of Monosulfoaluminate, in: Proceedings of the 31th Cem. Concr. Science Conference, London, England, 2011.

[10]. H. Pöllmann, T. Runcevski, R. Dinnebier, Synthesis and characterization of layered carbonated Calcium Aluminate Hydroxi Carbonate Hydrates, in: IV Int. Work Layered Materials, Campinas SP, Brazil, 2012.

[11]. H.F.W. Taylor, Cement Chemistry, second ed., Thomas Telford, London, 1997.

[12]. H.E. Schwiete, U. Ludwig, Crystal structures and properties of cement hydration products (hydrated calcium aluminates and ferrites), in: 5th ISCC, Vol 2, 1968, pp. 37-67.

[13]. H. Pöllmann, Characterization of Different Water Contents of Ettringite and Kuzelite, in: Proceeding of the XII Int. Congress on the Chemistry of Cement, Montreal, Canada, 2007.

[14]. W. Dosch, H. Keller, H. Strassen, 5th ISCC, Vol 2, 1968, pp. 72-77.

[15]. D. Damidot, F.P. Glasser, Thermodynamic investigation of the $CaO-Al_2O_3-CaSO_4-H_2O$ at 50°C and 85°C, Cem. Concr. Res. 22 (1992) 1179-1191.

[16]. I. Kaprálik, F. Hanic, Phase relations in the subsystem $C_4A_3\bar{S}$-$C\bar{S}H_2$-CH-H_2O of the system CaO-Al_2O_3-$C\bar{S}$-H_2O referred to hydration of sulphoaluminate cement, Cem Concr Res 19 (1989) 89-102.

[17]. H.J. Kuzel, Initial Hydration Reactions and Mechanisms of Delayed Ettringite Formation in Portland Cements, Cem. Concr. Compos. 18 (1996) 195-203.

[18]. H. Pöllmann, Die Kristallchemie der Neubildungen bei Einwirkung von Schadstoffen auf hydraulische Bindemittel, PhD Dissertation, University of Erlangen-Nuernberg, 1984.

[19]. M.H. Robert, Calcium Aluminate Hydrates and Related Basic Salt Solid Solutions, in: 5th ISCC, Vol 2, 1968, pp. 104-117.

[20]. R. Fischer, H.J. Kuzel, Reinvestigation of the system $C_4A{\cdot}nH_2O$ - $C_4A{\cdot}CO_2{\cdot}nH_2O$, Cem. Concr. Res. 12 (1982) 517-526.

[21]. M. Francois, G. Renaudin, O. Evrard, A Cementitious Compound with Composition $3CaO{\cdot}Al_2O_3{\cdot}CaCO_3{\cdot}11H_2O$, Acta Cryst. C54 (1998) 1214-1217.

[22]. T. Runcevski, R.E. Dinnebier, O.V. Magdysyuk, H. Pöllmann, Crystal structures of calcium hemicarboaluminate and carbonated calcium hemicarboaluminate from synchrotron powder diffraction data, Acta Cryst. B68 (2012) 493-500.

[23]. G. Renaudin, Y. Filinchuk, J. Neubauer, F. Goetz-Neunhoeffer, A comparative structural study of wet and dried ettringite, Cem. Concr. Res. 40 (2010) 370-375.

[24]. K.J. Parkinson, W. Day, Water Vapour Calibration using Salt Hydrate Transitions, J. Exp. Bot. 32 (1981) 411-418.

[25]. G.M. Richardson, R.S. Malthus, Salts for static control of humidity at relatively low levels, J. Appl. Chem. 5 (1955) 557-567,

[26]. I.M. Chou, R.R. Seal II, B.S. Hemingway, Humidity buffers and their application to the studies of dehydration reactions of sulfate salts at 0.1 Mpa, Am. Geophys., Union Trans. 79 (1998) S364.

[27]. I.M. Chou, R.R. Seal II, B.S. Hemingway, Determination of melanterite-rozenite and chalcanthite-bonattite equilibria by humidity measurements at 0.1MPa, Am. Mineral. 87 (2002) 108-114.

[28]. I.M. Chou, R.R. Seal II, Determination of epsomite-hexahydrite equilibria by the humidity-buffer technique at 0.1MPa with implications for phase equilibria in the system $MgSO_4$-H_2O, Astrobiology 3 (2003) 619-630.

[29]. I.M. Chou, R.R. Seal II, Determination of goslarite-bianchite equilibria by the humidity-buffer technique at 0.1MPa, Chem. Geol. 215 (2005) 517-523.

[30]. I.M. Chou, R.R. Seal II, Acquisition and Evaluation of Thermodynamic Data for Morenosite-Retgersite Equilibria at 0.1 MPa, Am. Mineral. 88 (2003) 1943-1948.

[31]. T. Matschei, Thermodynamics of Cement Hydration. PhD Dissertation, University of Aberdeen, 2007.

[32]. L. Greenspan, Humidity fixed points of binary saturated aqueous solutions, J. Res. Nat. Bur. Standards Sect. A 81 (1977) 89–96.

[33]. A. Le Bail, H. Duroy, J.L. Fourquet, Ab-initio structure determination of LiSbWO6 by X-ray powder diffraction, Mat. Res. Bull. 23 (1988) 447-452.

[34]. R. Allmann, Refinement of the hybrid layer structure $[Ca_2Al(OH)_6]^+ \cdot [1/2SO_4 \cdot 3H_2O]^-$, Neues Jb. Miner. Monat. (1977) 136-144.

[35]. J.F. Young, Humidity control in the laboratory using salt solutions – a review, J. Appl. Chem. 17 (1967) 241-245.

[36]. K. Linnow, Salt damage in porous materials: an XRD investigation, PhD dissertation, Universität Hamburg, 2007.

[37]. D.R. Williams, The characterisation of powders by gravimetric water vapor sorption, Int. Labmate. 20 (1995) 40-42.

[38]. L. Wadsö, A. Anderberg, I. Ålund, O. Söderman, An improved method to validate the relative humidity generation in sorption balances, Eur. J. Pharm. Biopharm. 72(1) (2009) 99–104

[39]. L. Wadsö, N. Markova, Comparison of three methods to find the vapor activity of a hydration step, Eur. J. Pharm. Biopharm. 51(1) (2001) 77-81.

[40]. L. Wadsö, N. Markova, A double twin isothermal microcalorimeter, Thermochim. Acta 360 (2000) 101-107.

[41]. L. Wadsö, N. Markova, A method to simultaneously determine sorption isotherms and sorption enthalpies with a double twin microcalorimeter, Rev. Sci. Instrum. 73 (2002) 2743-2754.

[42]. S.E.D. Hamad, A study of the reaction $Na_2SO_4 \cdot 10H_2O \rightarrow Na_2SO_4 + 10\ H_2O$ in the temperature range 0 to 25°C, Thermochim. Acta 17 (1976) 85–96.

[43]. P. Marliacy, R. Solimand, M. Bouroukb, L. Schuffenecker, Thermodynamics of crystallization of sodium sulfate decahydrate in H_2O-NaCl-Na_2SO_4: application to $Na_2SO_4 \cdot 10H_2O$-based latent heat storage materials, Thermochim. Acta 344 (2000) 85-94.

[44]. R. Espinoza, G. Scherer, Crystallization of sodium sulfate salts in limestone, Environ. Geol. 56 (2008) 605-621.

[45]. M.H. Fu, Z. Zhang, P.F. Low, Changes in the properties of a montmorillonite-water system during the adsorption and desorption of water: hysteresis, Clays Clay Miner. 38 (1990) 485-492.

List of Figures

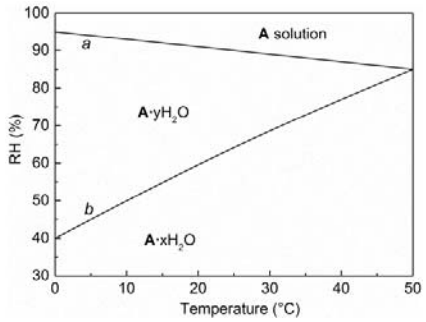

Fig. 1. RH/T phase diagram of the system A - H_2O

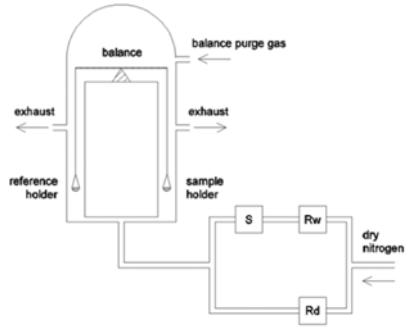

Fig. 2. Schematic picture of the sorption balance. Rw and Rd are mass flow controllers for the saturated and dry gas; S is the saturator

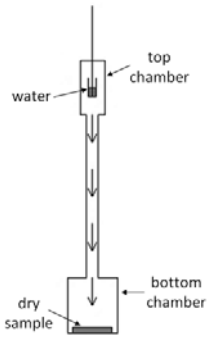

Fig. 3. Schematic graphic of the sorption ampoule. A dry sample is loaded in the bottom chamber and water is injected in the top chamber, where thermal power of sorption (P_{sorp}) and thermal power of evaporation (P_{vap}) are continuously measured by two twin microcalorimeters, respectively.

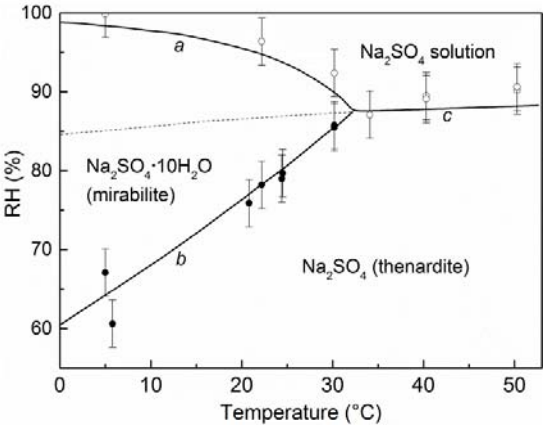

Fig. 4. RH/T phase diagram of the system $Na_2SO_4 + H_2O$ at 0.1 MPa (taken from Linnow [36]). The filled and open dots are our experimental results using the hydrate pair - humidity buffer method.

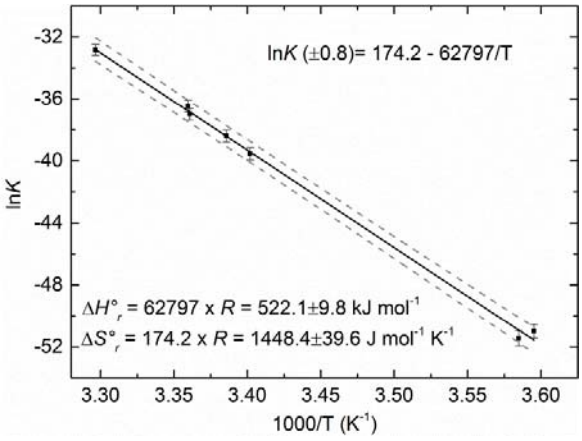

Fig. 5. Van't Hoff plot of our experimental results at different temperatures for reaction (7). Dashed line represents the 95% prediction band calculated with Origin Pro 8.5

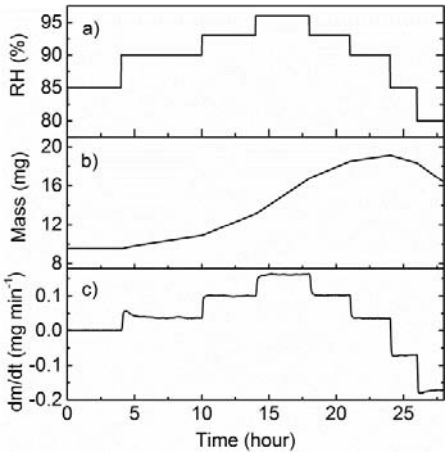

Fig. 6. a) RH step-wised program for the sorption balance. b) Mass change of sample. (c) dm/dt of sample.

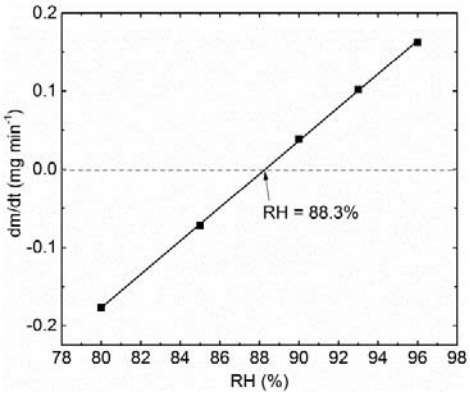

Fig. 7. Calculated RH of deliquescence of Na_2SO_4

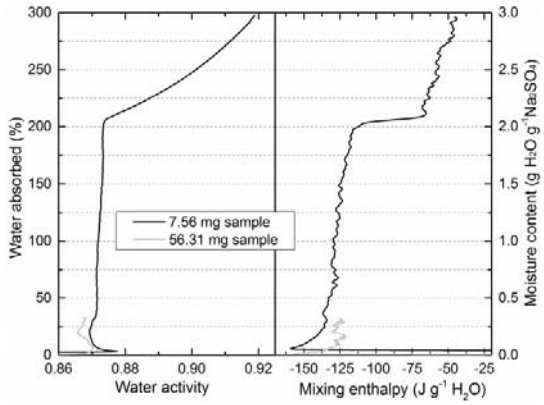

Fig. 8. The results of two measurements on thenardite with sorption calorimetry. The left diagram shows the sorption isotherm and the right one the mixing enthalpy as function of the moisture content (note that this graph is plotted with the mixing enthalpy on the x axis in order to compare it with the sorption isotherm graph). The y axes water absorbed and moisture content are proportional.

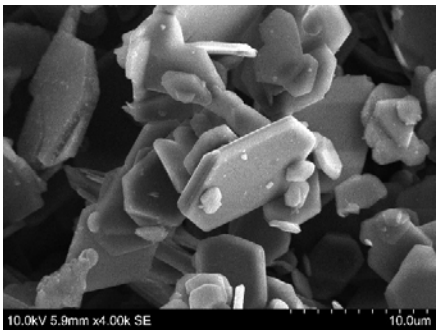

Fig. 9. SEM picture of monosulfoaluminate

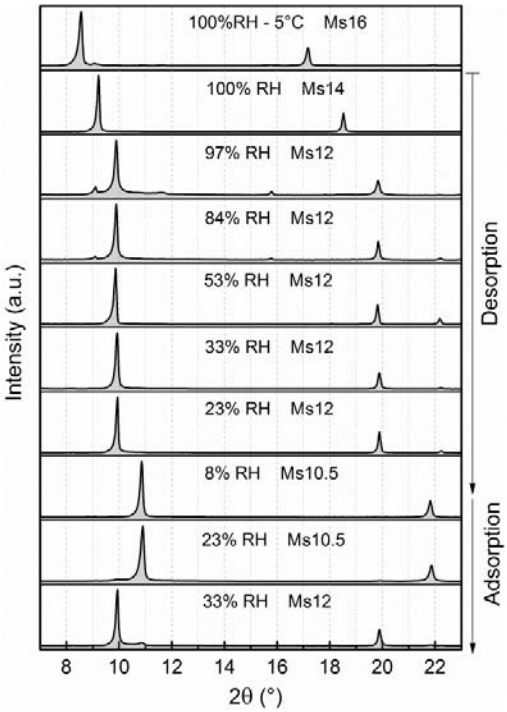

Fig. 10. XRD patterns of monosulfoaluminate dried at different RH at 25°C (unless otherwise stated)

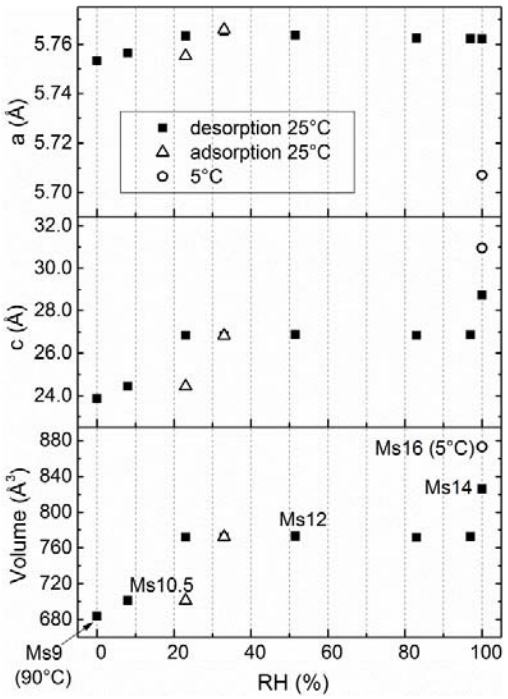

Fig. 11. Refined lattice parameter and volume of the lattice of monosulfoaluminate dried at different RH at 25°C (unless otherwise stated)

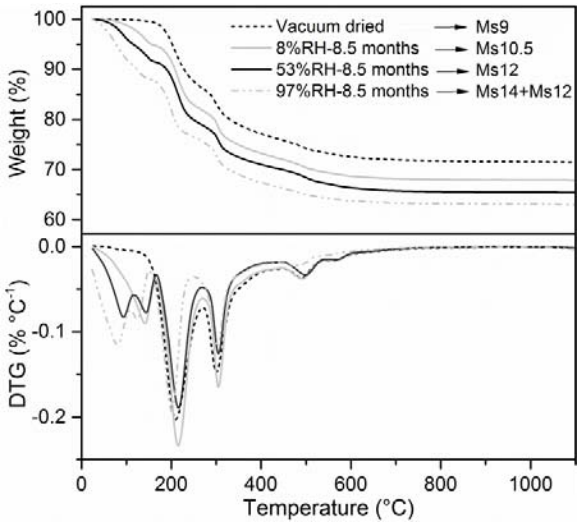

Fig. 12. TGA of monosulfoaluminate dried at different conditions at 25°C

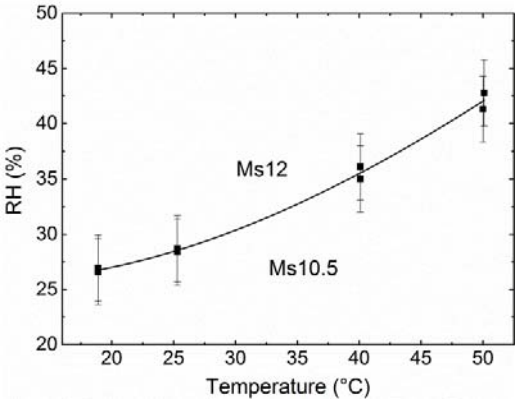

Fig. 13. Ms10.5-Ms12 equilibria at 0.1 MPa

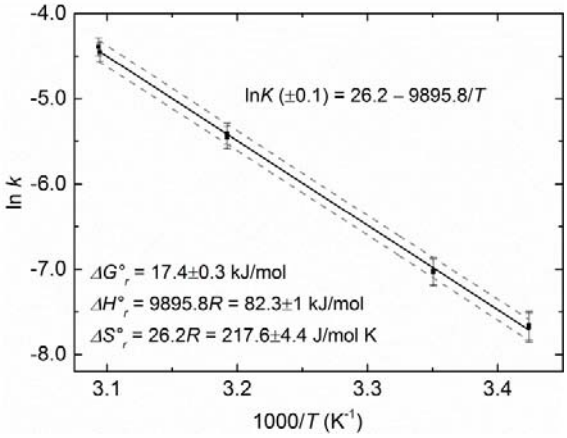

Fig. 14. Van't Hoff plot for Ms10.5-Ms12 equilibria. The dashed lines represent the 95% prediction band

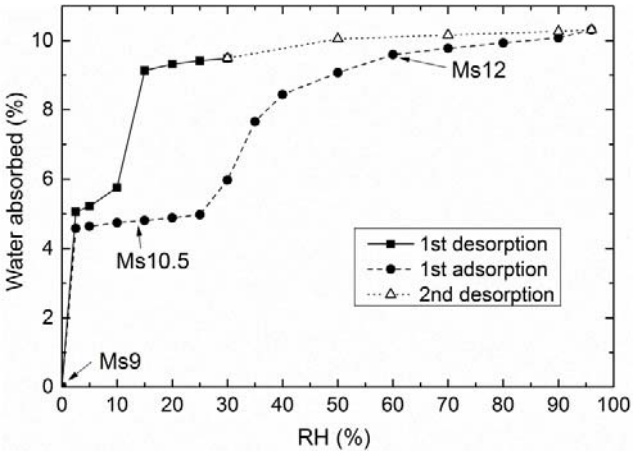

Fig. 15. Sorption isotherm of monosulfoaluminate at 25 °C

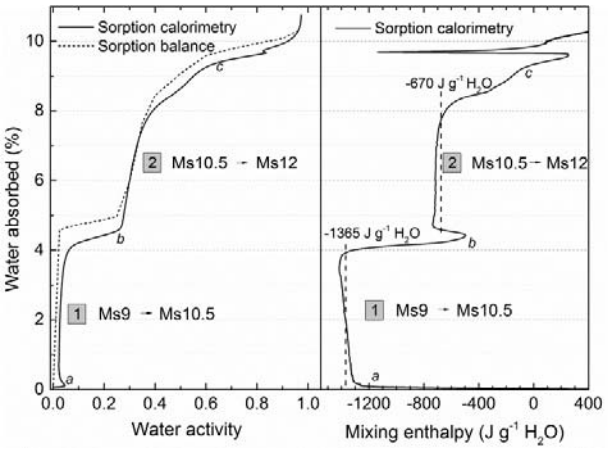

Fig. 16. Sorption calorimetry results on initially vacuum dried monosulfoaluminate at 25 °C. The left graph shows the calculated sorption isotherm (for comparison the isotherm obtained with sorption balance is superposed). The right graph presents the mixing enthalpy measured on the sample (the dashed lines represent the mean mixing enthalpies for the two observed processes)

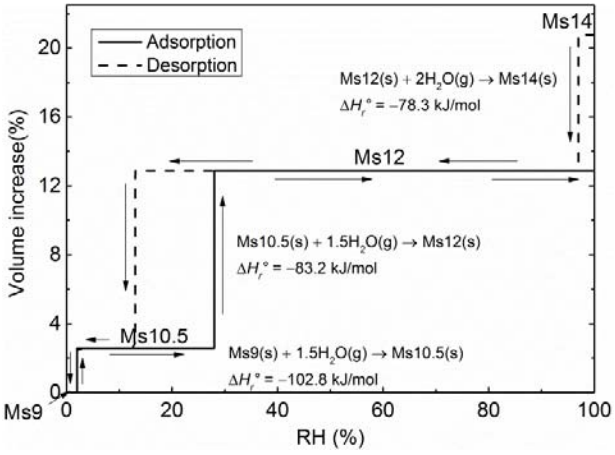

Fig. 17. Volume changes of monosulfoaluminate vs RH and related enthalpies of reaction at 25°C